ELSEVIER

PII: S1359-835X(98)00016-5

Composites Part A **29A** (1998) 1175–1183
1359-835X/98/$ - see front matter

Wettability, reactivity and stress relaxation of an NiAl(Ti)/Al_2O_3 composite

J. F. Silvain[a], J. C. Bihr[a] and J. Douin[b,*]
[a]*Institut de Chimie de la Matière Condensée de Bordeaux–CNRS, Université Bordeaux I, Château Brivazac, Av. Dr Schweitzer, 33608 Pessac, France*
[b]*Laboratoire d'Etudes des Microstructures, CNRS/ONERA, BP 72, 92322 Châtillon Cedex, France*

Sessile drop experiments, auger electron spectroscopy (AES) and transmission electron microscopy (TEM) analysis have been performed on composites: NiAl or NiAl(Ti) intermetallic matrix reinforced by α-alumina fibres. The role of Ti on the wettability behaviour at the fibre/matrix interface has been emphasized, as well as the reactivity of the fibre and the matrix during processing, and the effect of residual stress induced dislocations in the absence of NiAl and NiAl(Ti) cracks. © 1998 Elsevier Science Ltd. All rights reserved

INTRODUCTION

Studies on intermetallic materials are motivated by the need for high temperature materials for aeronautic and aerospace applications. The β-NiAl phase, which has an ordered bcc (B2) structure[1], is considered to be a suitable material for use at elevated temperature[2,3] due to its high melting temperature (1640°C), low density (5.86), and high Young's modulus (296 GPa) combined with excellent resistance to oxidation and thermal conductivity. The incorporation of pure alumina continuous fibres is proposed to overcome the disadvantages of this intermetallic, especially the lack of room-temperature ductility and toughness and low strength and creep resistance at high temperature.

The liquid route process used to manufacture this kind of composite requires a good knowledge of the wettability of the Ni–Al liquid alloy on the Al_2O_3 flat substrate, of the reactivity of the fibre with the matrix and of the accommodation of the stresses during the cooling stage.

- During the elaboration process, the first contact between the matrix and the fibre occurs in the liquid phase. The cohesion between fibre and matrix will be then very dependent on the good wettability of the matrix on the fibre substrate. Many studies have been done to evaluate the wettability behaviour of different metals (Ni and alloying Ni[4–7], Al[8], and different Ni–Al intermetallics[9]) on Al_2O_3 monocrystalline substrate, but there are no available data on NiAl and NiAl(+ alloying element).
- During processing and use of a composite, chemical reactions between the matrix and the fibre can occur, as well as diffusion of one element into the other. The knowledge of the reactivity behaviour of both elements is thus of prime importance to ensure cohesion at the interface and to control the degradation of the reinforcement. In particular, occurrence of new compounds created in the vicinity of or at the interface must be studied.
- Residual thermal stresses in metal–matrix composites result, during cooling, either from temperature gradients within the specimen or from a difference of coefficient of thermal expansion (CTE) between the constituents. The former effect can be controlled by a slow cooling rate. However, this slow cooling rate is in contradiction with the high cooling rate which is usually applied during metal–matrix composite (MMC) fabrication. In fact, a high cooling rate is required most of the time to minimize the fibre/matrix (F/M) interfacial reaction zone and to reduce grain growth within polycrystalline reinforcement[10–13]. Unless the CTEs of the constituents are identical or unless adaptive coatings are deposited on fibres in order to adjust CTE mismatch, MMC processing will thus always give rise to interfacial induced stresses. Usually, the larger contraction of the matrix compared to the reinforcement leads to tensile residual stresses in the matrix and to compressive residual stresses in the reinforcement. Since the fibres are always fragile, deformation must occur in the matrix in order to accommodate the CTE stresses during the processing. However, in certain circumstances, while the thermal induced stresses are very high, no cracks in the composite are observed, even for a fragile matrix. In such cases, the induced deformation must be accommodated somehow, either in the fibre or in the matrix.

* Corresponding author.

The aim of this work is to analyse the wettability and the reactivity behaviour of an Al_2O_3/NiAl and an Al_2O_3/NiAl(Ti) composite, and to characterize the interfacial dislocations which are induced during cooling in order to accommodate the stresses in the F/M zone close to the matrix. Sessile drop experiments and auger electron spectroscopy (AES) are used to point out the chemical interactions which take place at the F/M interface. The weak beam dark field microscopy technique is used to determine the Burgers vector, lines and glide planes of the different families of dislocations present in the vicinity of the F/M interface. A schematic model is proposed to understand how these dislocations accommodate the matrix strain and so avoid matrix cracks during processing.

EXPERIMENTS

Composite fabrication route

Alumina yarn. The fibre is polycrystalline and made of pure α-alumina. However, due to the pressure casting technique and the fusion temperature of NiAl, grain growth within alumina preform occurs. It has been shown[11] that above 1600°C and for a 1 h heat treatment the α-alumina grain size can reach the fibre diameter (see *Figure 1*) and thus α-alumina becomes a quasi single crystal.

NiAl matrix. Two intermetallic matrices were used in order to evaluate the influence of an additive element (Ti) on the wettability behaviour. The NiAl and NiAl + 1 at% Ti to 10 at% Ti alloys were obtained from pure Al, Ni and Ti powder (impurity concentration lower than 15 p.p.m.) of equivalent grain size (around 100 μm).

Infiltration procedure. A graphite crucible is first filled with the as prepared preform, then with the powder matrix and finally degassed inside the chamber. A high frequency coil heats the preform and the NiAl powder at the same time until the temperature reaches a few degrees above the melting point of the matrix. Once the matrix has melted and began to boil, the argon gas pressure is applied very smoothly. As soon as the maximum pressure is reached (30 bars), the induction heating is stopped. After the cooling of the matrix (360 s to reach 300°C) the pressure is removed[14].

Sessile drop experiments

Sessile drop experiments give values of the contact angle (θ) and the work of adhesion (W), or strength of interactions at the metal/fibre interface, knowing the surface tension of the liquid metal σ_{LV}. W is given by the Young–Dupre equation:

$$W = \sigma_{LV}(1 + \cos\theta)$$

Contact angle measurements were performed using the sessile drop method. The experiments were performed in a metallic molybdenum resistance furnace[15] under argon atmosphere purified by a sponge Ti getter in liquid nitrogen. Single crystal Al_2O_3 surfaces were mechanically polished, the average roughness was around 2 nm. The different Ni–Al alloys were prepared by argon arc melting before wetting experiments, and contained less than 15 p.p.m. metallic and oxygen impurities. Contact angles were measured directly from the image of the drop section with an accuracy of $\pm$ 2°.

AES and mathematical line scan treatment

The AES data were acquired on a MICROLAB 310-F Scanning Auger Microprobe which is mainly characterized by its Schottky field emission source of electrons which allows a high spatial resolution. This equipment also uses the spherical sector analysis to provide high energy resolution auger spectra. The depth resolution of the equipment is in the range of 1–3 nm.

The analysis conditions used for studying the composite samples were a voltage and beam current of 10 kV and 1 nA, respectively. The regions of interest for the analysis were in the range of 490–525 eV for oxygen, 1375–1415 eV for aluminium, 400–440 eV for titanium, and 820–870 eV for nickel. The data were recorded in the conventional EN(E) mode. A non-linear least-squared fitting treatment was applied on each of the 50 levels (1 point every 400 nm) and elemental chemical element enabled the atomic concentration versus position of each species to be found, according to their chemical environments.

Sample preparations and TEM observations

Thin slides were cut at a 45° angle with respect to the axis of the fibres and thinned by mechanical grinding to approximately 50 μm. Further thinning followed with an ion miller using a collimated beam of argon ions accelerated by a voltage of 6 kV. These thin slides were examined by conventional and weak beam TEM in a JEOL 200 CX microscope operating at 200 kV.

RESULTS AND DISCUSSION

Sessile drop experiments

Results. *Table 1* shows the results on contact angle

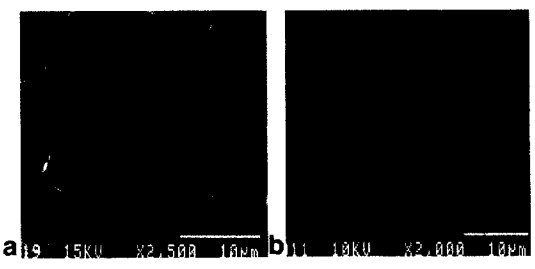

Figure 1 Scanning electron micrographs of an Al_2O_3 fibre section after annealing under argon atmosphere at: (a) 1600°C for 1 h; (b) 1750°C for 15 min

Table 1 Results of the sessile drop experiments for different Ni–Al alloys on monocrystalline α-alumina

Alloy/substrate	θ (°)	σ_{LV} (mJ mol^{-1})	W (mJ mol^{-1})	Bonding/rupture mode
NiAl/sapphire	80	1450	1701	Weak/adhesive
NiAl + 1 at% Ti/sapphire	80	1450*	1701	Strong/cohesive
NiAl + 2.5 at% Ti/sapphire	75	1450*	1825	Strong/cohesive
NiAl + 5 at% Ti/sapphire	70	1450*	1946	Strong/cohesive
NiAl + 10 at% Ti/sapphire	60	1450*	2175	Strong/cohesive

*Due to the absence of measured values and the high σ_{LV} of Ti[16] the σ_{LV} of NiAl(Ti) are set equal to the NiAl value.

Table 2 Results of the sessile drop experiments for different Ni–Al alloys on monocrystalline α-alumina

Alloy	θ (°)	σ_{LV} (mJ mol^{-1})	W (mJ mol^{-1})
Ni[17]	112	1750	1100
Ni_3Al[18]	83	1575	1760
NiAl	80	1450	1701
Al[19]	65	750	1070

measurements for different alloy–substrate systems. The contact angle values were measured under an argon atmosphere, but it has been verified that the values do not vary significantly with the furnace atmosphere (high vacuum, helium or inert gas). However, the kinetic of the drop spreading is much faster under a high vacuum atmosphere. The addition of titanium in NiAl has two effects: it decreases the contact angle (from 80° for NiAl to 60° for NiAl + 10 at% Ti) and changes drastically the bonding and rupture modes from weak and adhesive for the pure NiAl alloy to strong and cohesive for titanium-containing alloys. It can be noticed that for the same contact angle (80°), NiAl and NiAl + 1 at% Ti have different bonding behaviours. Nevertheless, for both alloy types, scanning electron micrographs of the sapphire substrate show rough surfaces and holes at the alloy location. After cooling, the surface drop of the different alloys has a shiny metallic aspect. As compared to other matt aspects for low Al amounts (Ni–0.03Al and Ni–0.08Al[9]) the metallic aspect indicates the absence of an oxide layer on the surface of the drop.

Discussion

Evolution of the surface drop during the sessile drop experiment. Due to the high chemical interactions between NiAl and NiAl(Ti) aluminium and the residual oxygen present inside the experimental chamber, a surface

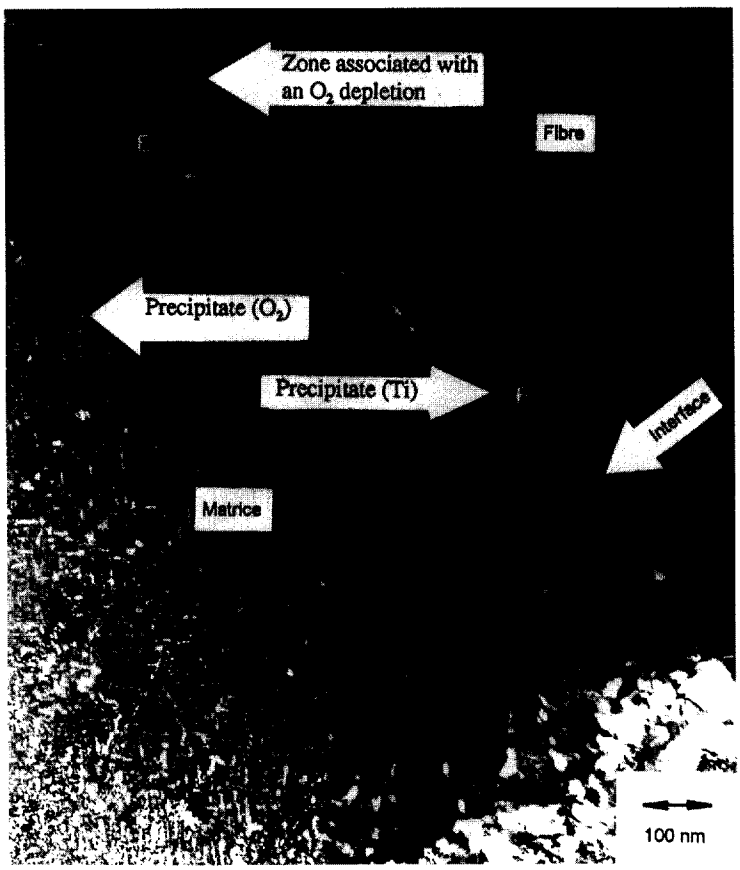

Figure 2 TEM dark field micrograph of NiAl(Ti)/Al_2O_3 interface

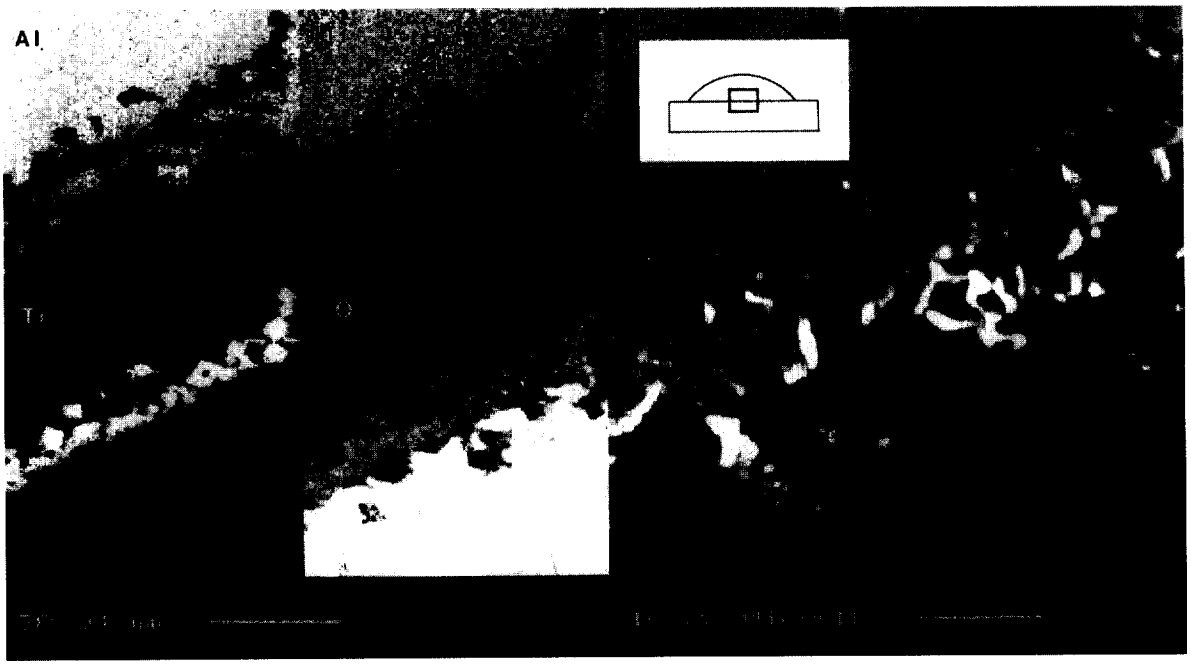

Figure 3 Cross-section electron probe micro analysis after sessile drop experiment of NiAl(2.5 at% Ti) on α-Al_2O_3 substrate

oxidation of the liquid drop occurs during the heating step. Then, dissolution equilibrium of both Al oxide, formed at the drop surface, and sapphire substrate lead to the following chemical reaction:

$$Al_2O_3(s) \rightarrow 2(Al)_{NiAl} + 3(O)_{NiAl} \quad (1)$$

eqn (1) shows that the dissolution of both the Al oxide surface of the liquid drop and the alumina substrate induce the presence of dissolved oxygen inside the alloy, at the drop surface and at the triple point. Therefore, at the liquid–vapour interface, this oxygen can react with the dissolved aluminium to form a volatile oxide leading to the deoxidation of the liquid drop. The chemical reaction is:

$$2(Al)_{NiAl} + (O)_{NiAl} \rightarrow Al_2O(g) \quad (2)$$

From eqns (1) and (2) the global chemical reaction which occurs during the sessile drop experiments and which explain the degradation of the sapphire substrate and the absence of oxide on the drop substrate can be written as follows:

$$Al_2O_3(s) + 4(Al)_{NiAl} \rightarrow 3Al_2O(g) \quad (3)$$

Evolution of the contact angle due to Ti addition. Even if the role of Al on the evolution of the contact angle has clearly been identified by various authors[9,15] and as it can be seen in *Table 2*, the effect, on the bonding strength or rupture behaviour of titanium additive element, is not clearly understood. TEM observation (cf. *Figure 2*) at the F/M interface shows evidence of crystalline precipitates at the F/M interface for the NiAl(Ti) matrix (points E and F). It has to be mentioned that these precipitates could not be crystallographically indexed due to their small size. However, the absence of that kind of interfacial precipitate for a NiAl/Al_2O_3 composite and the observation of Ti, at the F/M interface, by EPMA cartography on sessile drop experiments (cf. *Figure 3*), lead us to suggest that these precipitates should contain titanium. The different rupture mode observed during cooling, at the NiAl and NiAl(Ti)/Al_2O_3 interface, can be attributed to the presence of these precipitates which can act as nucleation sites during the cooling of the matrix. These sites, which are strongly bonded to the alumina fibres, enhance the adhesion properties, leading to a strong bonding and cohesive rupture mode of NiAl(Ti) on alumina.

It has to be pointed out that this is opposite to the work of Merlin and Eustathopoulos[9], which suggests that the weak bonding of Ni_3Al to Al_2O_3 is due to the absence of stress relaxation by plastic bonding. Stress relaxation is evidenced in our system (NiAl and NiAl(Ti)/Al_2O_3) and attributed to dislocation formations (see the next section).

Alloy/substrate chemical analysis on composite material

Results. *Figure 4(a)* and *(b)* shows the AES line profile (perpendicular to the fibre axis) across the NiAl(2% Ti)/Al_2O_3 interface. Three zones can be defined:

Zone A, in the fibre: The Al–O compound has a constant composition (O 60 at%, Al 38 at%) close to the nominal composition of the Al_2O_3 fibres. It has to be noticed that a slight diffusion of the NiAl(Ti) nickel and aluminium (*Figure 4(a)*) and of the NiAl(Ti) titanium (*Figure 4(b)*) occurs inside the fibre. This diffusion phenomenon is limited to the first micrometre fibre surface.

Zone B, the interface: The matrix/fibre interface zone is mainly characterized by a diffusion of the Al_2O_3 oxygen

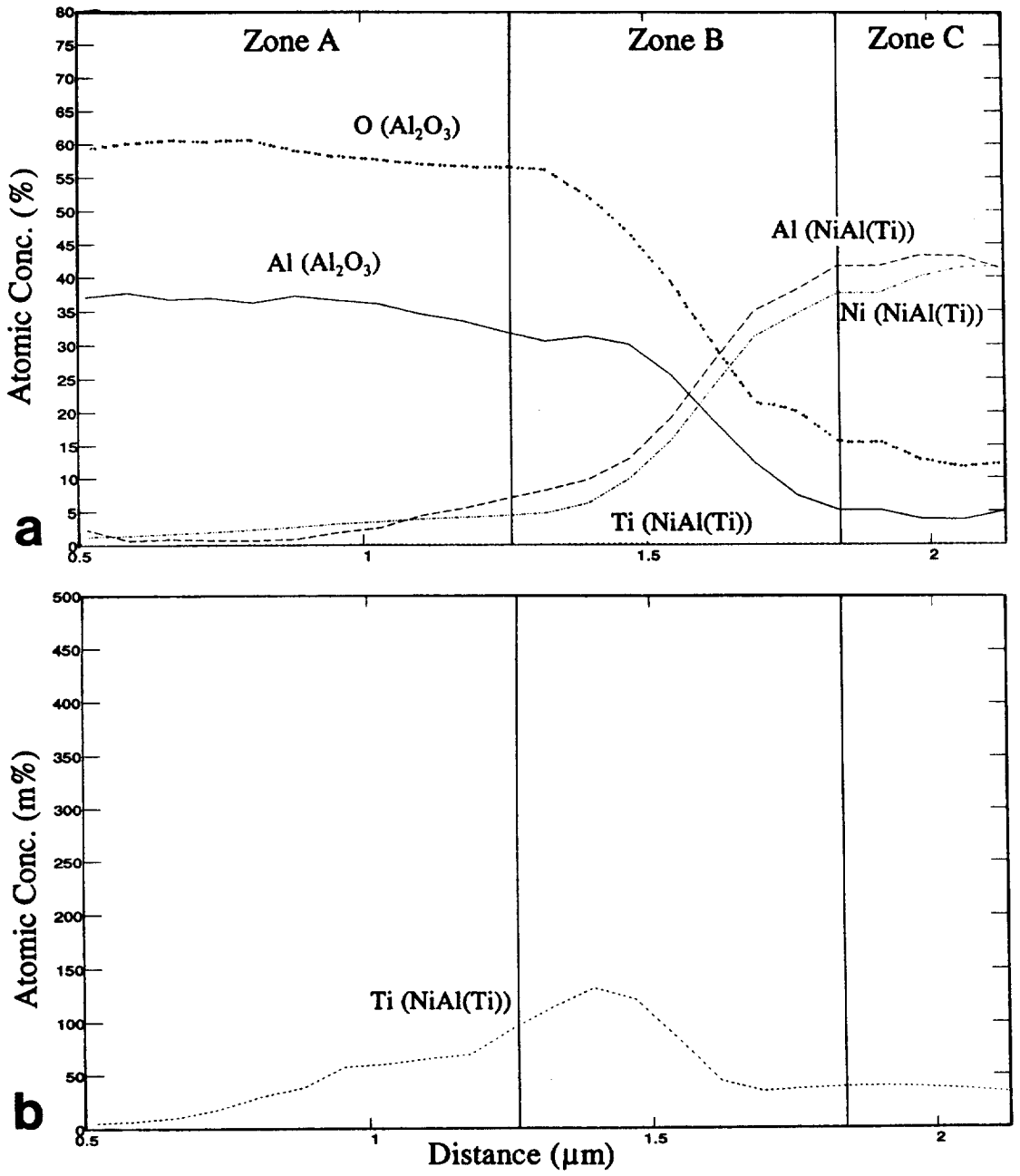

Figure 4 AES line profile across the NiAl(Ti)/Al_2O_3 interface

inside the NiAl(Ti) matrix and to a lesser extend of Al_2O_3 aluminium. Diffusion of aluminium, nickel and titanium atoms belonging to the NiAl(Ti) matrix inside the Al_2O_3 fibre can also be pointed out, but with a very small concentration, indicating that there is almost no diffusion of elements of the matrix in the fibre.

It is also important to notice that no reaction product is present in this interfacial zone. However, TEM observations at the F/M interfaces (cf. *Figure 2*) show evidence of numerous small crystalline precipitates in Ti-containing NiAl matrix, associated with an oxygen-depleted zone around the fibre.

Zone C, in the matrix: The NiAl(Ti) compound has a constant composition (Ni 42 at%, Al 42 at%, Ti 0.05 at%) close to the nominal composition of the matrix except for titanium (2 at%). The high amount of alumina oxygen (15 at%) which has also been directly observed by TEM[20] can be explained by thermodynamic considerations[14].

Discussions. The possible chemical interactions between the matrix and the fibre can be divided in two categories:

(1) the formation of a compound after reaction by either the matrix or the fibre with the other element, and/or
(2) the dissolution of one element inside the other.

As shown by AES experiments, there is no systematic formation of a new phase in the vicinity of the fibre and the

Table 3 Properties used in calculations (typical values from various sources); the coefficients of thermal expansion are given for an average temperature of 1000°C

	NiAl	Al_2O_3
Young's modulus (GPa)	250	320
Poisson's ratio	0.3	0.3
CTE ($\times 10^{-6}°C^{-1}$)	15.1	7
Fibre radius (μm)	—	5
Fibre volume fraction	—	44%

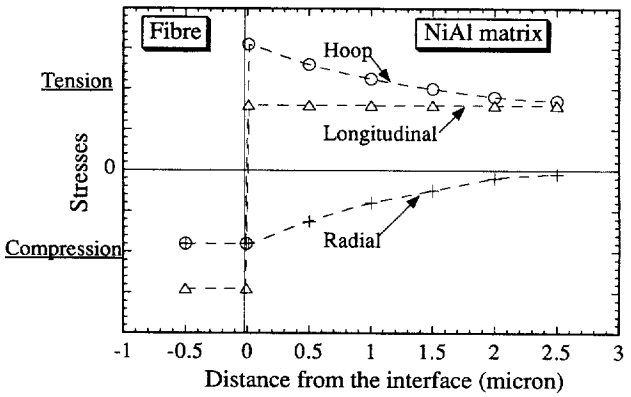

Figure 5 Schematic representation of the thermal induced stresses at the F/M interface

solubility of the matrix inside the fibre is very low. However, two types of precipitates are found at the F/M interface (titanium type precipitates points E and F, *Figure 2*) and in the matrix (oxygen type precipitates, *Figure 2*). Because of the O (Al_2O_3) diffusion inside the matrix, these matrix precipitates can be associated either to Al–O and/or to Ni–O species. If we now just consider the formation of the more probable oxide, NiO, calculations show that the chemical potential imposed inside the system and due to the alumina fibre, is too low to induce the formation of NiO. Thus, the dissolution of the alumina oxygen, inside the NiAl(Ti) matrix, will occur until the chemical potential reaches the value corresponding to the minimum oxygen pressure leading to the formation of alumina, and allowing the formation of Al–O type precipitates inside the NiAl(Ti) matrix.

Stress relaxation

Estimation of the residual stresses after cooling. The microstructure and more precisely the dislocation accommodations induced either by external or internal stresses are very important for the understanding of the behaviour of NiAl. A linear elastic model can simply be used to determine the residual stresses in the fibre and the matrix after cooling of the composite from the elaboration temperature (1800°C) to room temperature[14]. The different assumptions which have been done to calculate the residual stresses are as follows:

(1) The calculation has been done for a micro-composite having an isotrope, linear and elastic behaviour where the fibre and the matrix are considered as infinite in the axis direction. Thus, the different crystallographies and orientations of both the fibre and the matrix have not been taken into account.
(2) There is no temperature gradient inside the material and the system is always at equilibrium.
(3) The interphase area at the F/M interface is considered as ideal and the interfacial adhesion is strong.

Residual stresses were estimated using the characteristics of a α-Al_2O_3 single crystal and NiAl (*Table 3*) and the results of these calculations are schematically represented in *Figure 5*. Due to the simplified model which does not include stress relaxation by plastic deformation, the longitudinal and hoop stresses present a discontinuity at the interface while the radial stress appears more continuous. The model shows that after cooling, the fibre is in compression inside the composite whereas the matrix is in tension for axial and hoop stresses, while the matrix is in compression around the fibre leading to a clamping effect. Notice also that, because of the high fibre volume fraction used for this calculation (44%), the hoop and axial stresses do not tend to zero in the NiAl matrix as well as in the fibre. Finally, it has to be mentioned that a similar behaviour but with different magnitudes is obtained if we consider a cooling of the composite from 400°C (ductile-fragile temperature) to 20°C, or 1700°C (elaboration temperature) to 20°C.

Main characteristics of the dislocations in the matrix. In order to understand why there is no crack propagation during processing of the material while NiAl is known to be intrinsically fragile, especially at room temperature, we have studied the matrix microstructure.

As shown in *Figure 6* there is a high density of dislocations in the matrix in the vicinity of the fibre. In order to have a better, and simpler, understanding of the stress accommodation, we have chosen to study the vicinity of a fibre located within a single NiAl grain and parallel to the [1$\underline{1}$0] axis of the matrix. It should be pointed out that there exists a preferential growth of the matrix along this direction parallel to the fibre since a number of grains were found with this orientation.

The complete microstructural study shows that four different families of dislocations are present within the matrix: pure edge [110] dislocations parallel to the fibre axis, [001] and pure edge [1$\underline{1}$0] dislocations located around the fibre in the (110) plane perpendicular to the fibre axis, and [111] dislocations. Notice that as the TEM foils were prepared by cutting the sample at 45° with respect to the fibre axis, the cross-section of the fibre is an ellipsis with the edge [110] dislocations appearing, in projection, elongated along the axis of the ellipsis (see, e.g. *Figures 7* and *8*).

Accommodation of the residual stresses by dislocations. As schematically represented in *Figure 9*, [110] dislocations parallel to the fibre axis create supplementary half-planes

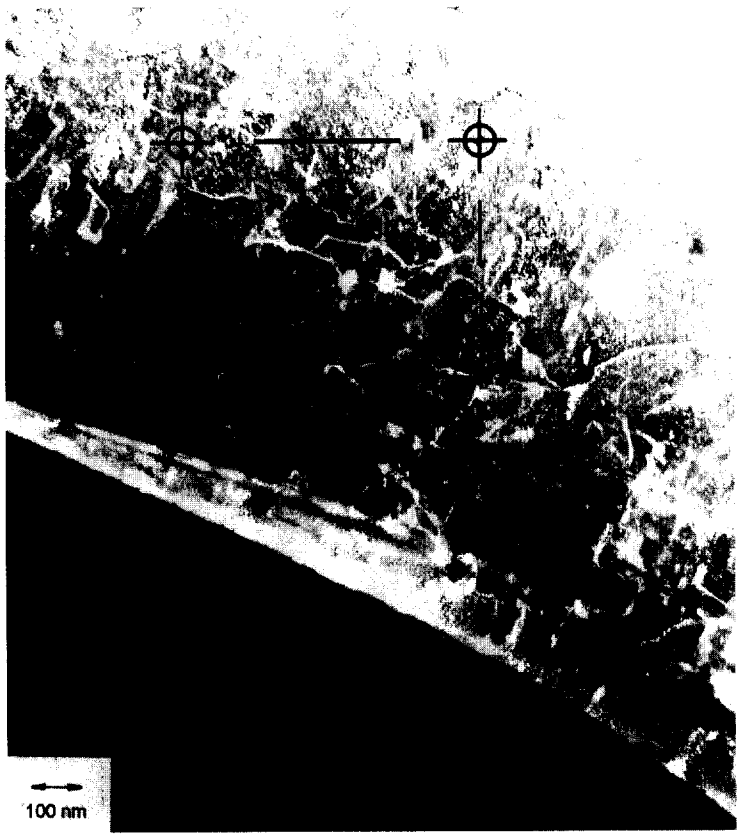

Figure 6 TEM dark field weak beam micrograph of the NiAl(Ti)/Al_2O_3 interface showing the different thermal induced stress dislocations

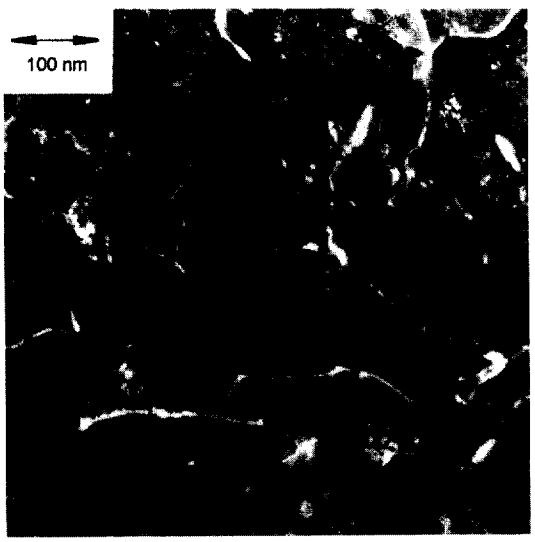

Figure 7 TEM dark field weak beam micrograph of the NiAl(Ti)/Al_2O_3 interface showing the different thermal induced stress dislocations (enlargement of *Figure 6*)

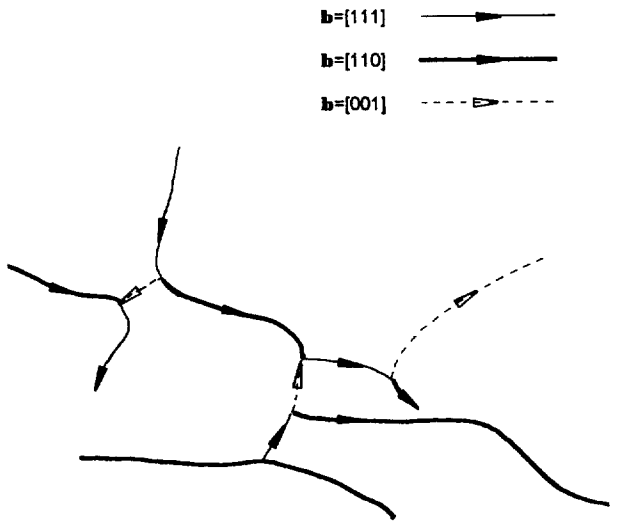

Figure 8 Schematic representation of the [111], [110] and [001] dislocations

which are inserted radially with respect to the fibre axis. These half-planes are ideally placed to accommodate the hoop stresses. This analysis remains true, but to a lesser extent, for the edge components of the [001] dislocations gliding in the (110) plane. Pure edge [1$\underline{1}$0] dislocations in the (110) plane also create supplementary half-planes which are perpendicular to the fibre axis. As shown in *Figure 10*, these half-planes contribute to the reduction of the longitudinal stress along the fibre axis. Finally, as the radial stress is the same for the fibre and the matrix at the interface, there is no need for interfacial dislocations in order to accommodate this stress.

Formation process of the dislocations. In NiAl, ⟨100⟩

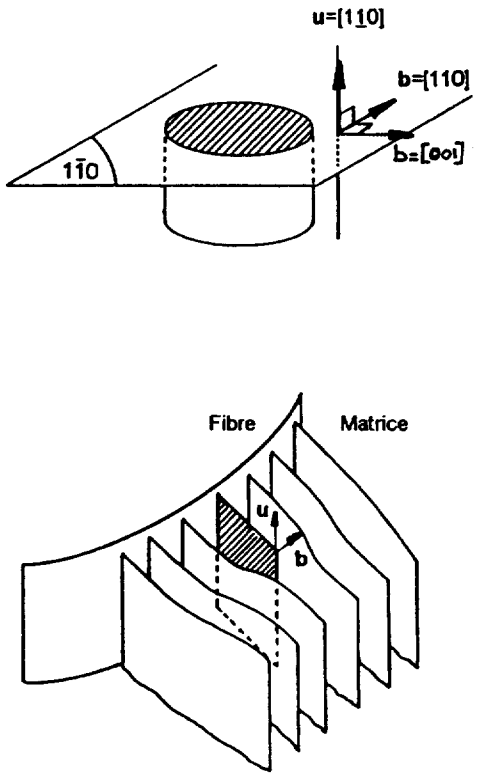

Figure 9 Accommodation of the hoop stress by creation of the $b = [110]$ and [001] dislocations

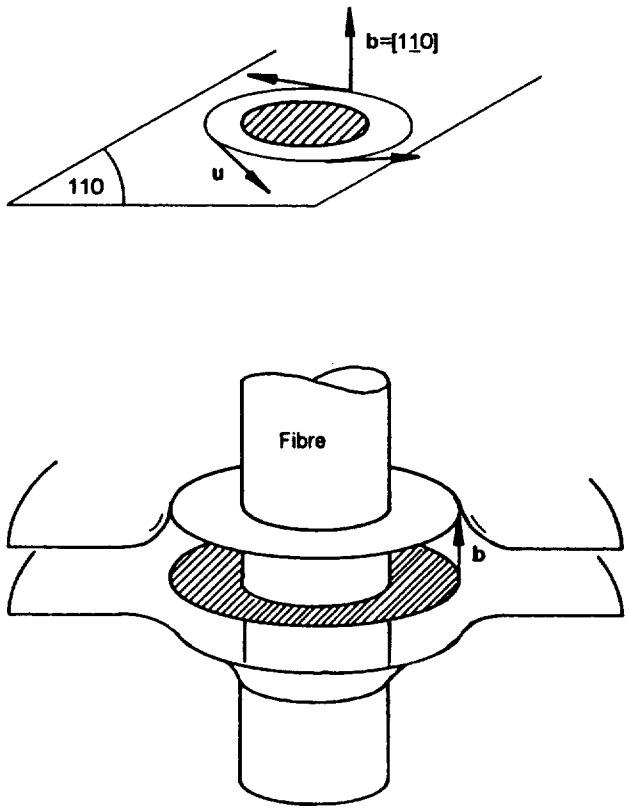

Figure 10 Accommodation of the axial stress by creation of the $b = [1\bar{1}0]$ dislocations

dislocations can be activated at every temperature when solicited along a ⟨100⟩ axis[21] and they are also the only dislocations which are not too difficult to activate at room temperature. However, if the deformation of NiAl only occurs by activation of ⟨100⟩ dislocations, this does not provide enough independent slip systems for plastic flow and the material appears fragile at room temperature. This is especially true when the activation of ⟨100⟩ dislocations is inhibited and ⟨111⟩ dislocations are then preferred in a crystal deformed in compression below 400°C. However, above the transition temperature (400°C), ⟨110⟩ dislocations begin to operate and the yield strength decreases sharply with temperature[22].

It is thus clear that during the first step of the cooling process, i.e. at high temperature, ⟨110⟩ dislocations, which are characteristic of the high temperature deformation of NiAl, are easily activated in such a way that they accommodate the temperature induced stresses. ⟨100⟩ dislocations can also be activated at high temperature but they appear to contribute less to the stress accommodation.

When the temperature drops down to 400°C, ⟨110⟩ dislocations are no longer activated and the accommodation of stress can only be obtained by formation of ⟨111⟩ dislocations. ⟨111⟩ dislocations are then activated either by direct formation in response to the residual stress or by interaction of [110] dislocations parallel to the fibre axis and [001] dislocations gliding in the (110) plane perpendicular to the fibre axis. The interaction:

$$[110] + [001] \rightarrow [111]$$

does not result in a gain in energy but in a gain in dislocation mobility as [111] dislocations are still mobile at lower temperatures.

CONCLUSION

Sessile drop experiment, auger electron spectroscopy and transmission electron microscopy analysis have been performed on NiAl, NiAl(Ti)/single monocrystalline α-alumina composites.

The use of these three methods enable us to emphasize the role of Ti on the wettability behaviour by cluster segregation at the F/M interface.

It has been shown that the dislocations found in the matrix are created during cooling of the composite in order to accommodate the residual stress due to the difference in CTE and allow the formation of crack-free composites.

REFERENCES

1. Field, R. D., Dobbs, J. R., Chang, K. M., Goldman, E. H. and Konitzer, D. G., *Ordered Intermetallics—Physical Metallurgy and Mechanical Behaviour*, eds. C. T. Liu, R. W. Cahn and G. Sauthoff. Kluwer Academic, The Netherlands, 1992, pp. 679–698.
2. Stoloff, N. S., *High-temperature Ordered Intermetallics Alloys, MRS Symp. Proc.*, Vol. 39, eds. C. C. Koch, C. T. Liu and N. S. Stoloff. MRS, Pittsburgh, Pennsylvania, 1985, pp. 3–27.

3. Stephens, J. R., *High-temperature Ordered Intermetallics Alloys, MRS Symp. Proc.*, Vol. 39, eds. C. C. Koch, C. T. Liu and N. S. Stoloff. MRS, Pittsburgh, Pennsylvania, 1985, pp. 381–395.
4. Kurkjian, C. and Kingery, W., *J. Phys. Chem.*, 1956, **60**, 961.
5. Armstrong, W. M., Charklader, A. C. D. and Clark, J. F., *J. Am. Soc.*, 1962, **45**, 115.
6. Ritter, J. E. Jr and Burton, M. S., *Trans. Am. Inst. Metall. Engrs*, 1967, **239**, 21.
7. Kritsalis, P., Merlin, V., Couturier, L. and Eustathopoulos, N., *Acta Metall. Mater.*, 1992, **40**, 1167.
8. Landry, K., Ph.D. thesis, Grenoble, France, 1995.
9. Merlin, V. and Eustathopoulos, N., *J. Mater. Sci.*, 1995, **30**, 3619.
10. Nourbakhsh, S. and Margolin, H., *Metall. Trans. A*, 1991, **22A**, 3059.
11. Silvain, J. F., Bihr, J. C., Le Petitcorps, Y. and Lahaye, M., *Advances in Sciences and Technology*, 1994, **7**, 719.
12. Jeng, S. M., Yang, J. M. and Amato, R. A., MRS Symp. Proc., 1992, **273**, 547.
13. Heintz, J. M., Bihr, J. C. and Silvain, J. F., *Key Engineering Materials*, 1997, **127–131**, 211.
14. Bihr, J. C., Ph.D. thesis, Bordeaux, France, 1996.
15. Naidich, Y., *Progress in Surface and Membrane Science*, 1981, **354**, 25.
16. Keene, B. J., *Int. Mater. Res.*, 1993, **38**, 157.
17. Champion, J. A., Keene, B. J. and Allen, S., *J. Mater. Sci.*, 1973, **8**, 423.
18. Bourreau, S., Ph.D. thesis, Grenoble, France, 1995.
19. Ayushima, G. D., Lewin, E. S. and Gel'd, P. V., Russian J. Phys. Chem., 1969, **43**, 1548.
20. Silvain, J. F. and Bihr, J. C., *J. Vac. Sci. Technol. A*, 1995, **13**(4), 1893.
21. Lahrmann, D. F. and Dorolia, R., *High-temperature Ordered Intermetallics Alloys IV, MRS Proc.*, Vol. 213, eds. L. Johnson, J. O. Stiegler and R. Pope, 1991, p. 603.
22. Miracle, D. B., Overview n°104. *Acta Metall. Mater.*, 1993, **41**(3), 649.